Supporting Information

New Insight into SPR Modulating by Two-Dimensional Correlation Spectroscopy: The Case for Ag/ITO System

Bingbing Han,[a] Sila Jin,[b] Qi Chu,[a] Yang Jin,[a] Xiangxin Xue,[a] Shuang Guo,[b] Yeonju Park,[c] Lei Chen[a,*] and Young Mee Jung [b,c,*]

[a]Key Laboratory of Preparation and Applications of Environmental Friendly Materials (Jilin Normal University), Ministry of Education, Changchun 130103, P.R. China

[b]Department of Chemistry, Institute for Molecular Science and Fusion Technology, Kangwon National University, Chunchon 24341, Korea

[c]Kangwon Radiation Convergence Research Support Center, Kangwon National University, Chunchon 24341, Korea

*To whom correspondence should be addressed.

E-mail: chenlei@jlnu.edu.cn (L.Chen); ymjung@kangwon.ac.kr (Y.M.Jung)

1. Experimental Section

1.1. Chemicals.

Ag and indium tin oxide (ITO) targets with a purity of 99.99% were purchased from Beijing TIANRY Science & Technology Development Center and Beijing Jingmai Zhongke Material Technology Co., Ltd., respectively. Polystyrene (PS) microspheres (200 nm, 10% w/w) were purchased from Bangs Laboratories Inc. All chemicals were used without further purification.

1.2. Assembly of the PS colloidal sphere array.

Two-dimensional (2D) ordered templates were prepared by a self-assembly method.[1-4]

(1). Cut the silicon/glass substrate to a suitable size, then place the silicon/glass substrate in a 6:1:2 volume ratio of H_2O, NH_4OH and H_2O_2 mixed solution heated to 300 °C, and keep it under these conditions for 5-10 min. Pour out the mixed solution after cooling. Then, use deionized water and anhydrous ethanol to alternately ultrasonically clean the substrate 3 times.

(2). Use a volume ratio of PS pellets to absolute ethanol of 1:1. Apply ultrasound for 1 min to mix them thoroughly. Use a pipette to drop an appropriate amount of mixed liquid onto a large silicon wafer. Then, tilt the large silicon wafer, and steadily dip it into a basin filled with water that has a stable surface. Driven by the water current, the small balls on the silicon wafer form a single-layer ordered array of colloidal balls on the water surface.

(3). Use the cleaned small silicon/glass substrate to slowly pick up the monolayer film on the water surface, and use filter paper to absorb excess water.

Finally, a 2D close-packed colloidal sphere array with a periodic structure is formed on the silicon/glass substrate.

1.3. Preparation of the composite nanomaterial substrate.

Ag and ITO arrays were fabricated on the microspheres or glass by using a magnetron sputtering system (ATC 1800-F): Use mechanical pumps and molecular pumps to obtain a 2×10^{-4} Pa vacuum in the sputtering chamber, and adjust the flapper valve so that the working pressure is 0.6 Pa, where the gas flow is 20 sccm and the sputtering gas is high-purity argon. Adopt the layer-by-layer sputtering method; first, sputter the

Ag layer, and then, sputter the ITO layer. Use a sputtering power for Ag of 10 W, a sputtering rate of 10 nm/min, and a sputtering time for all samples of 1 min. Use a sputtering power for ITO of 100 W and a sputtering rate of 5 nm/min. The ITO layer thickness can be changed by controlling the sputtering time.

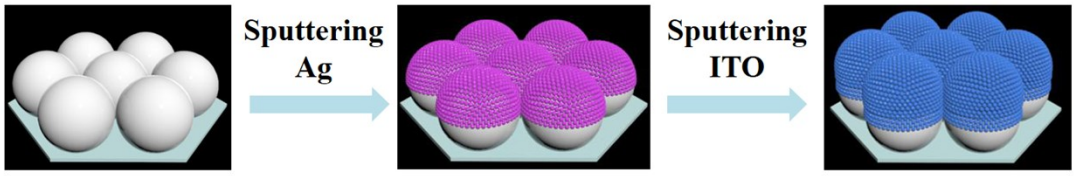

Scheme 1. Schematic of the fabrication process of the Ag/ITO@PS ordered arrays.

1.4. Characterization of the composite nanomaterial substrate.

To explore the morphology and microstructure of the Ag/ITO arrays, a JEOL 6500F scanning electron microscope (SEM) operating at an accelerating voltage of 200 kV was used. Energy dispersive X-ray spectroscopy (EDS) measurements were also performed using the SEM linked with an Oxford Instruments X-ray analysis system. Ultraviolet-visible (UV-vis) absorption spectra were obtained using a Shimadzu UV-3600 plus spectrometer. X-ray photoelectron spectroscopy (XPS) spectra were recorded using a Thermo Scientific ESCALAB 250Xi A1440 system. The carrier density of the Ag/ITO film was tested by a Hall effect detector (Lakeshore, 775HMS Matrix).

1.5. 2D-COS based on UV-vis-NIR spectra.

The series of the UV-vis-NIR spectra the Ag/ITO samples obtained with different carrier densities, which is a set of dynamic spectra, is transformed in a set of 2D correlation spectra by simple cross-correlation analysis. 2D-COS calculation was carried out using homemade code in MATLAB R2019b (the MathWorks Inc., Natick, MA, USA).

The mathematical derivation of 2D-COS is provided.[5-7] $A(\nu_j,t_k)$ is an obtained set of spectra for the measured system under the influence of an applied external perturbation that induces spectral intensity changes. In our system, the spectral variable ν_j with $j = 1, 2, \ldots n$ is the wavelength, and the other variable t_k with $k = 1, 2, \ldots m$ denotes the

effect of the applied external perturbation (ITO thickness time indicating the carrier density of Ag/ITO systems).

$\tilde{A}(\nu_j,t_k)$ is the dynamic spectra used in 2D correlation spectroscopy, which is defined as

$$\tilde{A}(\nu_j,t_k) = \begin{cases} A(\nu_j,t_k) - \bar{A}(\nu_j) & for\ 1 \le k \le m \\ 0 & otherwise \end{cases} \quad (1)$$

where, $\bar{A}(\nu_j)$ is the reference spectrum of the system. The reference spectrum is usually the averaged spectrum over the observation interval between t_1 and t_m.

$$\bar{A}(\nu_j) = \frac{1}{m}\sum_{k=1}^{m} A(\nu_j,t_k) \quad (2)$$

Synchronous and asynchronous 2D correlation spectra, $\Phi(\nu_1,\nu_2)$ and $\Psi(\nu_1,\nu_2)$, are given by

$$\Phi(\nu_1,\nu_2) = \frac{1}{m-1}\sum_{j=1}^{m} \tilde{A}(\nu_1,t_j)\cdot\tilde{A}(\nu_2,t_j) \quad (3)$$

$$\Psi(\nu_1,\nu_2) = \frac{1}{m-1}\sum_{j=1}^{m} \tilde{A}(\nu_1,t_j)\cdot\sum_{i=1}^{m} N_{ij}\tilde{A}(\nu_2,t_i) \quad (4)$$

The term N_{ij} is the element of the so-called Hilbert-Noda transformation matrix.[8]

The synchronous 2D correlation spectrum $\Phi(\nu_1,\nu_2)$ indicates that the spectral intensity changes for the two different spectral variables, ν_1 and ν_2, occur simultaneously.

In a synchronous 2D correlation spectrum, the autopeaks and cross-peaks appear on the diagonal line and in the off-diagonal line, respectively. Autopeaks show overall spectral intensity changes induced by an applied external perturbation. The cross-peaks represent coincidental or simultaneous spectral intensity changes observed at two different spectral variables. A positive cross-peak represents that two spectral intensities are increasing or decreasing together, while a negative cross peak indicates that one is increasing and the other is decreasing. Therefore, intra- or inter-molecular interactions from correlations between two different spectral variables can be detected.

The corresponding asynchronous 2D correlation spectrum $\Psi(\nu_1,\nu_2)$ depicts the out-of-phase or sequential changes in spectral intensities. It shows dissimilarity of spectral intensity changes of two different spectral variables. In the asynchronous 2D correlation spectrum, only cross-peaks are observed, which occur when two spectral intensities at ν_1 and ν_2 change out of phase with each other. Therefore, the overlapped bands corresponding to the spectral signals from different origins can be clearly resolved.

Interestingly, from the analysis of 2D correlation spectra, the sequential order of the intensity changes observed under the external perturbation can be determined. If the signs of the cross-peaks in synchronous and asynchronous 2D correlation spectra are the same, the intensity changes at ν_1 occur before those at ν_2. In contrast, if the signs of the cross-peaks are different, the intensity changes at ν_1 occur after those at ν_2.

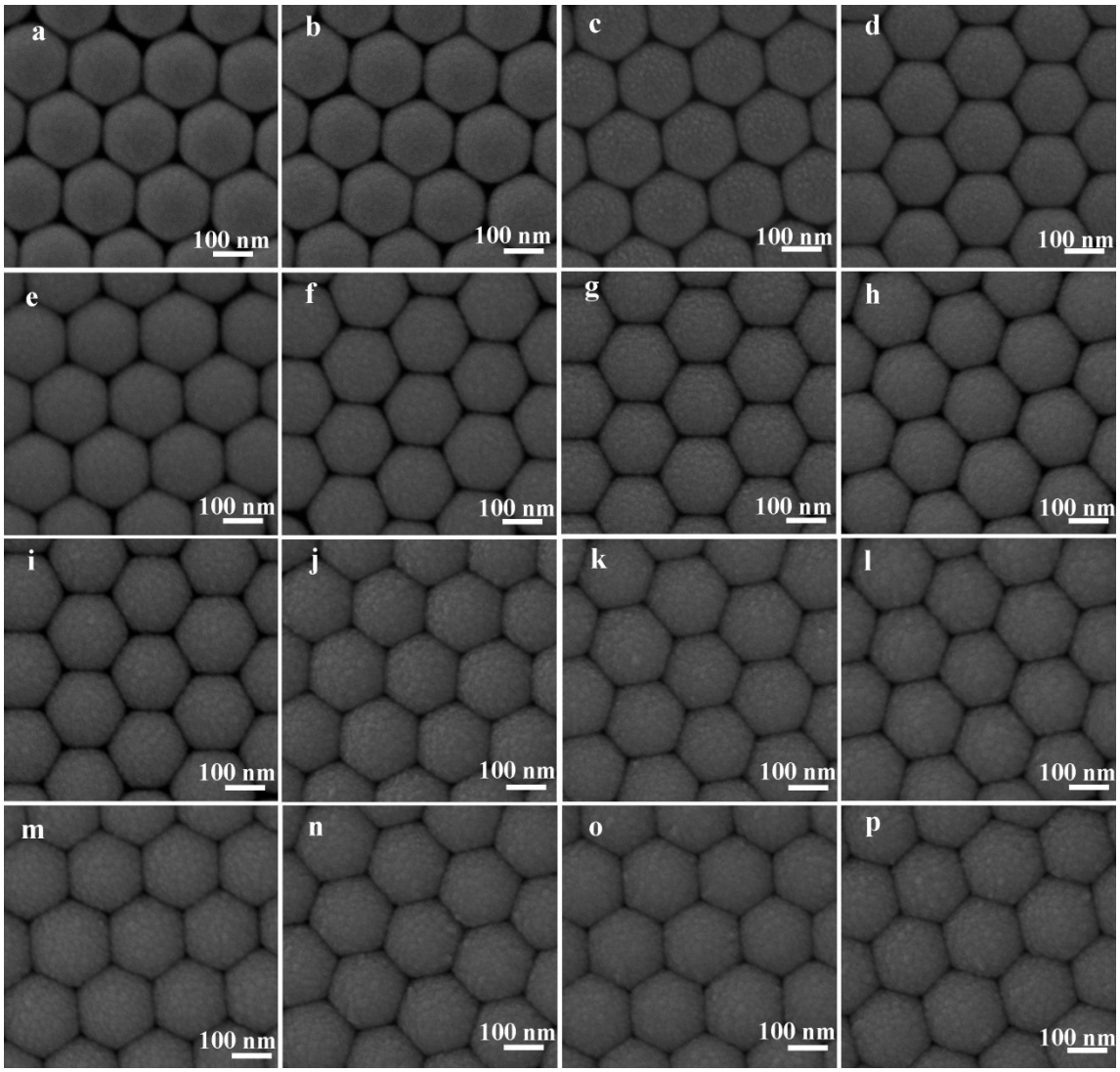

Fig. S1. (a)~(o) SEM images of Ag/ITO films sputtered on the PS template; the bottom layer is a Ag film with a sputtering thickness of 10 nm. The top layer is an ITO layer with a sputtering thickness of 0 to 140 nm. (P) SEM image of a pure ITO film with a thickness of 140 nm sputtered on the PS template.

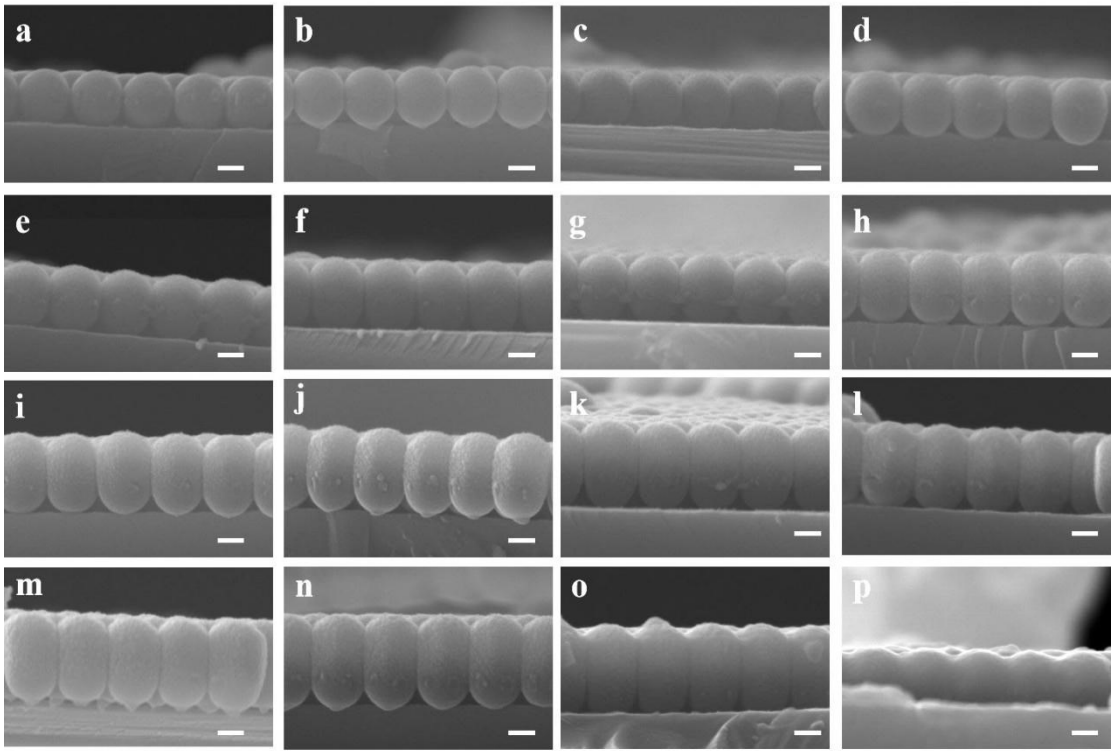

Fig. S2. SEM cross-sectional views corresponding to Fig. S1 a ~ p. The scale bars are all 100 nm.

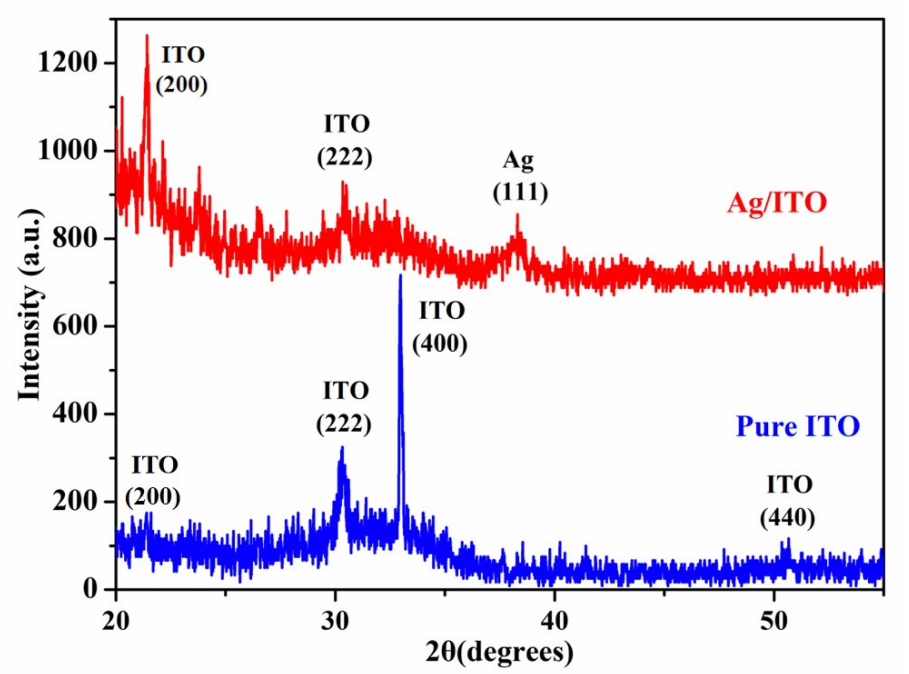

Fig. S3. X-ray diffraction (XRD) patterns of Ag-10 nm/ITO-10 nm (red line) and ITO-10 nm (blue line).

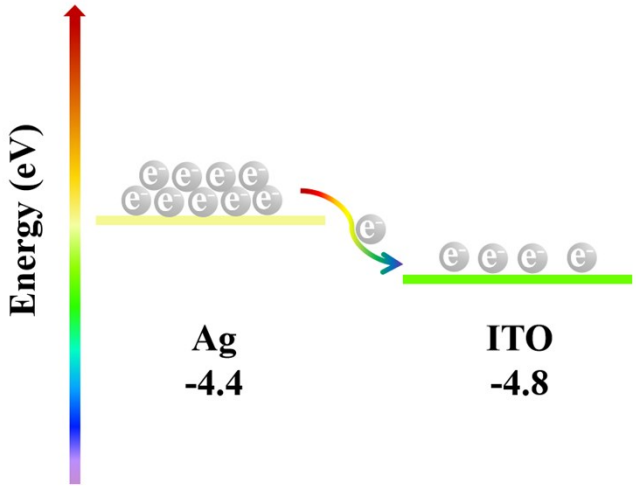

Fig. S4. The energy level diagrams of Ag/ITO heterojunction.

Table S1. Carrier density and Hall mobility detected by the Hall effect system (the results shown in the table are the median average of 4 test values) The sputtering thickness of Ag for all samples is 10 nm, and "x" represents the sputtering thickness of the ITO layer, ranging from 0 to 140 nm

Ag-10/ITO-x (nm)	Carrier density (cm^{-3})	Hall mobility ($cm^2 \cdot V^{-1} \cdot s^{-1}$)
0	3.94×10^{22}	7.64×10^{-3}
10	2.59×10^{22}	1.40×10^{-2}
20	4.98×10^{21}	4.03×10^{-2}
30	1.52×10^{21}	8.28×10^{-2}
40	3.93×10^{20}	9.04×10^{-2}
50	2.58×10^{20}	2.91×10^{-1}
60	5.40×10^{19}	6.07×10^{-1}
70	2.84×10^{19}	7.91×10^{-1}
80	1.51×10^{19}	8.94×10^{-1}
90	6.67×10^{18}	1.12
100	6.31×10^{18}	2.16
110	5.40×10^{18}	2.37
120	5.33×10^{18}	4.73
130	4.98×10^{18}	1.64×10^{1}
140	4.20×10^{18}	4.64×10^{1}
Pure ITO film 140 nm	1.67×10^{18}	5.96×10^{1}

Table S2. Assignments of the absorbance peaks of the layer-by-layer sputtered Ag/ITO@PS films

Number	Wavelength (nm)	Peak assignments[9-17]
L_1	560	The α resonance mode of Ag@PS hemispherical shell structure
L_2	594	L_1 affected by the ITO film
L_3	823	Weaker in-plane quadrupole resonances of Ag
L_4	848	L_3 affected by the ITO film
L_5	1115	The β resonance mode of the Ag@PS hemispherical shell structure
L_6	2102	LSPR of the ITO film
L_7	2121	LSPR of the coupled ITO and Ag films
L_8	1181	L_5 affected by the ITO film

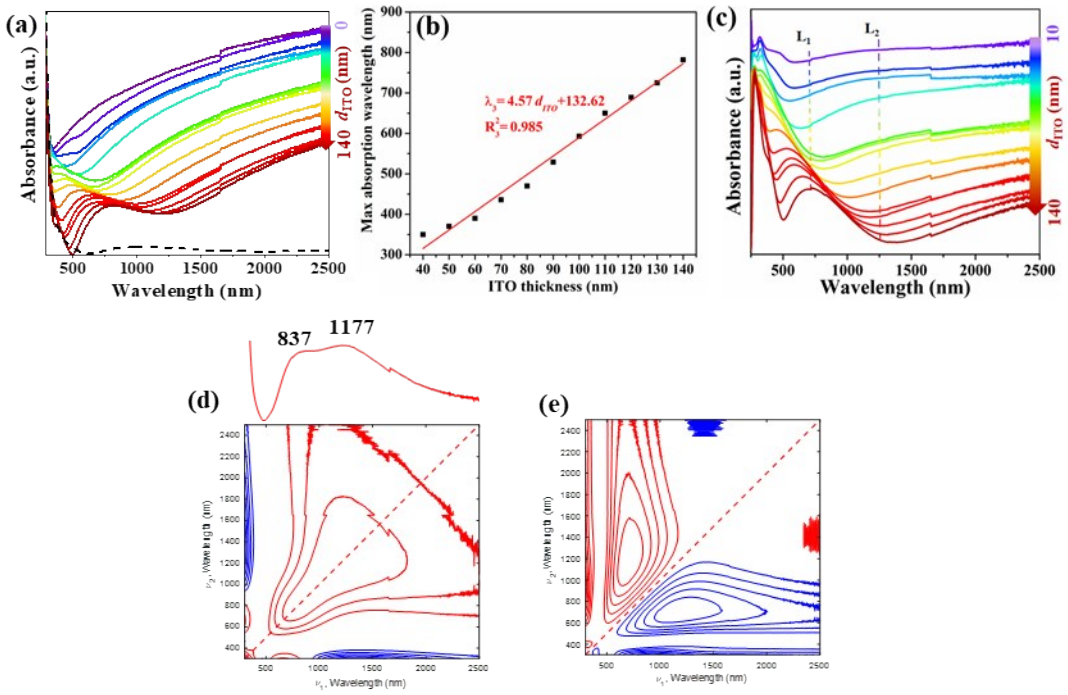

Fig. S5. (a) UV-vis-NIR absorption spectra of Ag/ITO films sputtered on glass; the bottom layer is a Ag film with a sputtering thickness of 10 nm; the top layer is an ITO layer with a sputtering thickness of 0 to 140 nm. (b) Linear relationship between the maximum absorption wavelength and the ITO layer thickness fitted according to the data in (a). (c) Absorption spectrum obtained by subtracting the Ag@glass spectrum from the absorption spectrum in (a). (d) Synchronous and (e) asynchronous 2D correlation spectra calculated from the UV-vis-NIR absorption spectrum in (a). Red and blue lines in the 2D correlation spectra represent positive and negative cross peaks, respectively.

The number of extinction peaks that a metal nanoparticle can produce depends on how many polarization modes can be excited by the excitation light. Compared with the hemispherical shell of the Ag/ITO@PS array, the spherical Ag NPs in the Ag/ITO@glass system exhibit only one absorption peak at a short wavelength. Fig. S5a shows the absorption spectra of the Ag/ITO system sputtered on a glass surface. The thickness of Ag on the bottom layer is 10 nm, and the thickness of ITO on the top layer is 0~140 nm. The maximum absorption wavelength depends on the ITO layer thickness

(Fig. S5b). The correlation is 0.985, indicating that the LSPR is strongly dependent on the ITO layer thickness without the PS template. By controlling the ITO layer thickness, the LSPR in the visible region can be accurately tuned. From the perspective of the carrier density, as the carrier density decreases, the LSPR is continuously redshifted, and the peak intensity becomes stronger. 2D-COS was also used to analyze the dependence of the peak displacement on the carrier density changes. Synchronous and asynchronous 2D correlation spectra are shown in Figure S5 d and e, respectively. The synchronous cross peak at (1248, 704) nm is positive, which shows that the decreasing intensities of the peaks at 704 and 1248 nm are assigned to Ag-related absorbance. The 2D correlation spectral analysis suggests that the absorption peak at 704 nm shifts before that at 1248 nm during the decrease in the carrier density. As shown in the subtracted spectra in Figure S5c, the half-width of the absorption peak at 704 nm is significantly reduced, indicating that the absorption peak at this position is attributable to the LSPR generated by the strong coupling between Ag NPs and ITO NPs. The absorption peak at 1248 nm monitored by 2D-COS obviously disappears, indicating that the absorption peak at this position is attributable to the LSPR generated by the coupling between Ag NPs. The changes in the absorption peak of Ag and ITO NPs precede those of Ag NPs, indicating that carriers are first applied to the Ag-ITO interface. Thus, 2D-COS analysis of the dependence of each component in the UV-vis-NIR spectrum on the carrier density response is a very reliable method for exploring the carrier transport process.

References

1. X. Y. Zhang, D. Han, N. Ma, R. Gao, A. Zhu, S. Guo, Y. Zhang, Y. Wang, J. Yang, and L. Chen, *J. Phys. Chem. Lett.,* 2018, **9**, 6047-6051.

2. B. Han, S. Guo, S. Jin, E. Park, X. Xue, L. Chen, and Y. M. Jung, *Nanomaterials,* 2020, **10**,1455.

3. X. Y. Zhang, D. Han, Z. Pang, Y. Sun, Y. Wang, Y. Zhang, J. Yang, and L. Chen, *J. Phys. Chem. C,* 2018, **122**, 5599-5605.

4. N. Ma, L. Chen, T. Jing, X.-Y. Zhang, B. Han, X. Xue, Y. Zhang, and B. Zhao, *J. Phys. Chem. C,* 2019, **123**, 28846-28851.

5. I. Noda and Y. Ozaki, *Two-Dimensional Correlation Spectroscopy - Applications in Vibrational and Optical Spectroscopy*, John Wiley & Sons, Ltd, Chichester, UK, 2004.

6. Y. M. Jung and I. Noda, *Encyclopedia of Analytical Chemistry*, John Wiley & Sons, Ltd, Chichester, UK, 2018, 1-27.

7. Y. Park, I. Noda, and Y. M. Jung, *Front. Chem.,* 2015, **3**, 1-16.

8. I. Noda, *Appl. Spectrosc.,* 2000, **54**, 994-999.

9. M. Cortie and M. Ford, *Nanotechnology,* 2007, **18**, 235704.

10. C. X. Wang, W. D. Ruan, N. Ji, W. Ji, S. Lv, C. Zhao, and B. Zhao, *J. Phys. Chem. C,* 2010, **114**, 2886-2890.

11. A. I. Maaroof, M. B. Cortie, and N. Harris, *Small,* 2010, **4**, 2292-2299.

12. S. Larson and Y. P. Zhao, *J. Phys. Chem. C,* 2018, **122**, 7374-7381

13. Z. Zhan, R. Xu, and Y. Mi, *ACS Nano*, 2015, **9**, 4583-4590.

14. S. Larson, Z. Yang, and Y. Zhao, *Chem. Commun.,* 2019, **55**, 1342-1344.

15. G. Garcia, R. Buonsanti, and E. L. Runnerstrom, *Nano Lett.,* 2011, **11**, 4415-4420.

16. M. Kanehara, T. Yoshinaga, and T. Teranishi, *J. Am. Chem. Soc.,* 2009, **131**, 17736-17737.

17. G. V. Naik, V. M. Shalaev, and A. Boltasseva, *Adv. Mater.,* 2013, **25**, 3264-3294.